Decondensation in Nonequilibrium Photonic Condensates: When Less Is More

Henry J. Hesten, Robert A. Nyman,* and Florian Mintert
Quantum Optics and Laser Science Group, Blackett Laboratory, Imperial College London, Prince Consort Road, London SW7 2BW, United Kingdom

(Received 5 May 2017; published 23 January 2018)

We investigate the steady state of a system of photons in a pumped dye-filled microcavity. By varying pump and thermalization the system can be tuned between Bose-Einstein condensation, multimode condensation, and lasing. We present a rich nonequilibrium phase diagram which exhibits transitions between these phases, including decondensation of individual modes under conditions that would typically favor condensation.

DOI: 10.1103/PhysRevLett.120.040601

Phase transitions in systems governed by quantum statistics at thermal equilibrium have been investigated intensely. Canonical examples of these transitions are the formation of Cooper pairs in the superconductivity transition [1], or the transition of a thermal cloud of bosonic atoms to a Bose-Einstein condensate (BEC) as temperature decreases [2,3]. The study of nonequilibrium phase transitions has spanned many disciplines from classical physics to social sciences [4], and explained many phenomena, such as trends in society [5] or traffic jams [6]. Only recently has attention turned to nonequilibrium phase transitions in quantum systems. For example, the condensation of polaritons in semiconductor [7–9] or organic [10,11] solids has been observed outside thermal equilibrium. Dynamical and nonequilibrium quantum phase transitions are among the most impressive experimental uses of quantum simulators, using trapped atoms [12], trapped ions [13,14] and NMR qubits [15]. Driven-dissipative many-particle quantum systems showing intricate phase diagrams [16,17] and bistability phenomena giving rise to coexisting phases have also been observed [18], including using superconducting qubits [19].

Our system of study is a gas of photons confined in a dye-filled microcavity which, when the dye is pumped, can be made to thermalize and Bose-Einstein condense [20,21], as predicted by thermal-equilibrium theory. Thermalization results from absorption and reemission of light from the cavity by the dye [22], which is limited by emission from the cavity [23,24]. Thermal equilibrium is thus always imperfect and breaks down completely if the cavity is far detuned from the dye molecular resonance [25,26]. The system then features multimode condensation [24,27,28] as a clear signature of nonequilibrium behavior. It has been noted that multimode systems driven far from equilibrium can show multimode condensation [29], and that the kinetics of two-mode laser systems can be made to show a sort of minimalist Bose-Einstein condensation [30,31].

Extrapolating from prior experiments on nonequilibrium phase transitions [17,19], one would expect that condensation is always favored by an increase in the pump rate [7,20] and a decrease in thermalization rate. This is typically true for the overall fraction of photons in condensed modes. For individual modes, however, we also find the opposite behavior in the regime far out of equilibrium. That is, modes with condensed photons can lose their macroscopic occupation as the pump rate is increased, which is similar to decreasing entropy as temperature increases or negative heat capacities [32]. This gives rise to a highly complex dependence of the steady state on properties like pump rate, geometry, and the time scale of thermalization.

We employ a model [25] that has been derived from a fully quantized microscopic description of a dye-filled cavity, which is applicable to a wide range of systems which need only satisfy a few criteria: an optical environment with a well-defined ground state, a fluorescent gain medium, and rescattering of light faster than loss resulting in thermalization. We predict the dependence of multimode condensation on such properties, and despite the nonlinear nature of the system we find analytic laws characterizing condensation and decondensation that coincide accurately with numerically exact solutions.

In dye-filled microcavities only one longitudinal mode of the harmonic cavity is sufficiently close to resonance with the dye molecules; the dynamics can then be reduced to a two-dimensional model with transverse modes labeled by $m = [m_x, m_y]$. Taking into account loss through the mirrors and spontaneous emission from dye molecules into modes that are not confined within the cavity results in the well-established equation of motion [24]

$$\frac{dn_m}{dt} = -\kappa n_m + \rho\Gamma_{\downarrow}^{(m)} f_m(n_m + 1) + \rho\Gamma_{\uparrow}^{(m)}(f_m - 1)n_m, \quad (1)$$

for the average occupation n_m of mode m, where κ is the cavity decay constant, $\Gamma_{\uparrow}^{(m)}$ and $\Gamma_{\downarrow}^{(m)}$ are, respectively, the

rates of absorption from and emission into mode m, and ρ is the areal density of molecules; f_m is the fraction of excited molecules interacting with mode m, and it is given in terms of the fraction $f(\mathbf{r})$ of molecules at point $\mathbf{r}$ which are excited and the mode profile $\psi_m(\mathbf{r})$ via the relation $f_m = \int d^2\mathbf{r} f(\mathbf{r})|\psi_m(\mathbf{r})|^2$. The dynamics of the excited-state population is governed by

$$\frac{\partial f(\mathbf{r})}{\partial t} = -\Gamma_{\downarrow}^{\mathrm{tot}}(\mathbf{r}) f(\mathbf{r}) + \Gamma_{\uparrow}^{\mathrm{tot}}(\mathbf{r})[1 - f(\mathbf{r})], \qquad (2)$$

in terms of the rates of total absorption and emission, $\Gamma_{\downarrow}^{\mathrm{tot}}(\mathbf{r})$ and $\Gamma_{\uparrow}^{\mathrm{tot}}(\mathbf{r})$, which depend on the mode occupations via

$$\Gamma_k^{\mathrm{tot}}(\mathbf{r}) = \Gamma_k(\mathbf{r}) + \sum_m |\psi_m(\mathbf{r})|^2 \Gamma_k^{(m)}(n_m + \delta_{k\downarrow}), \qquad (3)$$

with $k = \uparrow, \downarrow$ and $\delta_{\uparrow\downarrow} = 1 - \delta_{\downarrow\downarrow} = 0$, where $\Gamma_{\uparrow/\downarrow}(\mathbf{r})$ are the pump rate of molecules by the laser, and the decay of molecules not captured by emission into the modeled cavity modes.

As the thermalization process occurs when excitations are exchanged between cavity modes and dye molecules, we compare the rate of absorption $\rho\Gamma_{\uparrow}^{(m)}$ to the rate of loss κ and define the thermalization coefficient $\gamma = \rho\Gamma_{\uparrow}^{[0,0]}/\kappa$ [33]. We choose parameter values appropriate to real experiments, but specify all values in units of cavity decay κ (which for typical experiments is of the order of 10^9/s) and harmonic oscillator length L (the mean spatial extent of the lowest cavity mode). The shape of absorption and emission profiles $\Gamma_{\uparrow/\downarrow}^{(m)}$ for the individual modes are extracted from experimental data [34] and their peaks are set to $1.2 \times 10^{-9}\kappa$ (see Supplemental Material [35]). We consider a slightly anisotropic cavity with mode spacings $\omega_x = \omega_y/1.01 = 3 \times 10^4\kappa$, and a detuning between the molecular resonance frequency and the lowest cavity eigenfrequency ranging from $-3.5 \times 10^5\kappa$ to $-1.89 \times 10^5\kappa$. The pump of the molecules of areal density $\rho = 10^{12}/L^2$ has a Gaussian profile with width $20L$, and the decay rate $\Gamma_{\downarrow}$ of excited molecules is set to $\Gamma_{\downarrow} = \kappa/4$. The anisotropy of the cavity is chosen in order to avoid degeneracies, but it is sufficiently small so that mode pairs $[m_x, m_y]$ and $[m_y, m_x]$ behave almost identically, and their condensation thresholds are hardly distinguishable. We will therefore only discuss modes $[m_x, m_y]$ with $m_x \leq m_y$. In order to arrive at a finite-dimensional problem, we consider cavity modes with $m_x + m_y \leq 6$ only.

Figure 1 (top panel) depicts the stationary solutions for mode occupations as functions of pump rate, and one can see steplike increases and decreases of the populations, i.e., condensation and decondensation of individual modes at specific values of pump rate. The BEC phase is defined by

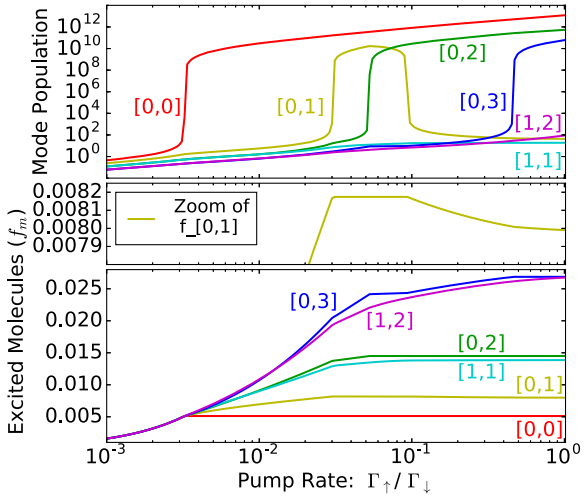

FIG. 1. The upper panel depicts the mode populations n_m as functions of pump rate for a constant thermalization rate $\gamma = 1.8$. One can clearly see how mode [0, 1] condenses and then decondenses with increasing pump rate. The lower panel depicts the fraction of excited molecules f_m accessible to any mode, and substantiates that the decondensation of mode [0, 1] is congruent with a decrease of $f_{[0,1]}$. This is highlighted in the central panel, which is a magnification of the lower panel.

condensation in the lowest cavity mode only, whereas a multimode condensate contains additional condensed modes. Any phase with one or more condensed modes but an uncondensed ground mode is considered a laser [37], and any phase without any condensed modes will be called uncondensed. With increasing pump rate, Fig. 1 (top panel) thus features the transition from an uncondensed phase to BEC, followed by a transition from BEC to a multimode condensate, and three transitions between different multimode condensates.

Despite the system's complex, nonlinear behavior, we can develop an understanding of (de)condensation in terms of the decomposition of the total pump rate into individual contributions given in Eq. (3). For low populations n_m of all modes, the total rates of absorption and emission can be well approximated by direct pumping and loss; i.e., Eq. (3) reduces to $\Gamma_{\uparrow/\downarrow}^{\mathrm{tot}}(\mathbf{r}) \simeq \Gamma_{\uparrow/\downarrow}(\mathbf{r})$, so that the pumping of dye molecules [Eq. (2)] is proportional to the external pumping. In the case of strongly occupied modes, on the other hand, the approximation $\Gamma_{\uparrow/\downarrow}^{\mathrm{tot}}(\mathbf{r}) \simeq \sum_m |\psi_m(\mathbf{r})|^2 \Gamma_{\uparrow/\downarrow}^m n_m$ in terms of the rates $\Gamma_{\uparrow/\downarrow}^m n_m$ of stimulated absorption and emission holds, and the proportion of excited dye molecules is largely independent of external pumping but depends mostly on the interaction with the condensed mode or modes. Molecules in spatial domains where $|\psi_m(\mathbf{r})|^2 \Gamma_{\uparrow/\downarrow}^m n_m \gg \Gamma_{\uparrow/\downarrow}(\mathbf{r})$ are thus clamped to mode m.

As pumping is increased, the excitation of unclamped molecules grows. In particular, uncondensed modes thus experience a growing reservoir of excitations that can help them to gain enough population to condense. As a mode

condenses it also starts to clamp dye molecules and the number of molecules clamped to this mode grows with increasing population n_m. This mode thus enters a competition for access to excitations with the other modes. Since the excitation of molecules that are clamped to a condensed mode is approximately independent of the external pump, an initially condensed mode does not benefit from this increase in pump. Such a mode is thus likely to lose the competition and decondense. This effect can be explicitly seen in the fraction of excited molecules $f_{[0,1]}$ accessible to mode [0, 1] as shown in Fig. 1 (center and bottom panels). $f_{[0,1]}$ increases below the condensation threshold of mode [0, 1]; but as clearly visible in the center panel, $f_{[0,1]}$ becomes independent of the pump exactly at threshold. This clamping mechanism survives the onset of the condensation of mode [0, 2], but as the population of mode [0, 2] grows, the fraction of excited molecules $f_{[0,1]}$ accessible to mode [0, 1] decreases. Quite strikingly, this decrease is rather minute and visible only in the magnified panel. Nevertheless, it has an extremely significant impact and results in decondensation of mode [0, 1].

With this qualitative understanding of decondensation at hand, we can now proceed to a quantitative prediction of condensation thresholds; a more detailed analysis and the explicit analytic solutions can be found in the Supplemental Material [35]. The mode population n_m for stationary solutions to Eq. (1) diverges if f_m approaches the critical value

$$f_m^c = \frac{\Gamma_\uparrow^{(m)} + \frac{\kappa}{\rho}}{\Gamma_\downarrow^{(m)} + \Gamma_\uparrow^{(m)}}. \tag{4}$$

Neglecting contributions from uncondensed modes to the total pump rate [Eq. (3)], one obtains the stationary solutions

$$f_m^{(s)} = \int d^2\mathbf{r} |\psi_m(\mathbf{r})|^2 \frac{\Gamma_\uparrow^{\mathrm{tot}}(\mathbf{r})}{\Gamma_\uparrow^{\mathrm{tot}}(\mathbf{r}) + \Gamma_\downarrow^{\mathrm{tot}}(\mathbf{r})} \tag{5}$$

of Eq. (2) for *all* modes as functions of the mode populations n_m of the *condensed* modes. Gain clamping implies the condition $f_m^s \lesssim f_m^c$ for the condensed modes, which, in turn determines n_m for all condensed modes. This permits identification of pump rates (or other system parameters) that achieve the condensation condition for an originally uncondensed mode. The thresholds for Bose-Einstein condensation, multimode condensation, and the decondensation of mode [0, 1] while mode [0, 2] is condensed are depicted as white lines in the phase diagram depicted in Fig. 2.

The accuracy of these estimates can be verified by comparisons to numerically exact solutions. The steady-state solution of Eq. (1), together with Eq. (5), can be found with algebraic root-finding routines, and we verified explicitly that the obtained solutions coincide with the solutions obtained by propagation until a stationary state is reached. Defining phase boundaries can be done unambiguously in the thermodynamic limit, but it poses an intricate problem in systems of finite size. Since numerically exact solutions do not result in diverging mode populations, we employ large increases in the population of a single mode under small changes of driving conditions [as depicted in Fig. 1 (top panel)] as indicators of condensation threshold [7,27]. Quantitatively, we define the threshold of condensation (decondensation) as an increase (decrease) in

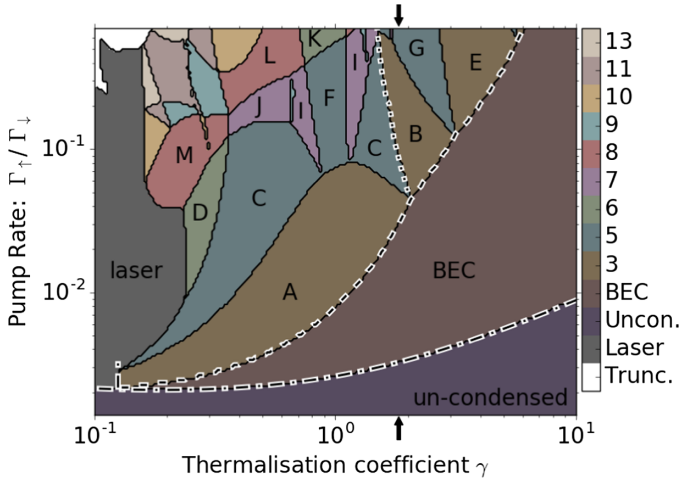

	Condensed modes
BEC	[0,0]
A	[0,0] [0,1]
B	[0,0] [0,2]
C	[0,0] [0,1] [0,2]
D	[0,0] [0,1] [0,2] [1,1]
E	[0,0] [0,3]
F	[0,0] [0,1] [0,3]
G	[0,0] [0,2] [0,3]
I	[0,0] [0,1] [0,2] [0,3]
J	[0,0] [0,1] [0,2] [0,4]
K	[0,0] [0,1] [0,3] [2,2]
L	[0,0] [0,1] [0,2] [0,4] [2,2]
M	[0,0] [0,1] [0,2] [1,1] [0,3]

FIG. 2. Phase diagram of the photon gas as function of pump rate $\Gamma_\uparrow$ and thermalization coefficient γ. Different colors indicate the number of condensed modes with the sole exceptions of "laser," which indicates condensed phases of the system without condensation in the ground mode, and "truncated," indicating potential truncation errors as the highest considered mode has condensed. Capital letters indicate which modes are condensed in a given region. Narrow areas in which only one of modes $[m_x, m_y]$ and $[m_y, m_x]$ are condensed are treated as if both modes are condensed in order to avoid structures that are too detailed; the fine structures between regions I and J and adjacent to region M are a result of this. Rough phase boundaries in the top left region are due to limited numerical accuracy. The analytic estimates for various phase transitions indicated by white lines coincide very accurately with the numerically obtained thresholds. The cut for $\gamma = 1.8$ through the phase diagram depicted in Fig. 1 is indicated by bold arrows.

population greater than 3 orders of magnitude over an increase in pump rate of 10%, but due to the sharp nature of all observed transitions, the identification of threshold is largely independent of the explicitly chosen numerical values [35].

As depicted in Fig. 2 the system at lower pump rates is in the uncondensed phase, with no condensed modes. At large thermalization coefficient and pump rate the system is in the BEC phase. As the thermalization coefficient is decreased from here, the system passes through various multimode phases, until the ground mode is no longer condensed. Under these conditions the system behaves like a laser, where condensation is a consequence of stimulated emission, rather than a condensate, for which absorption and emission play equally important roles. The trend that strong pumping and weak thermalization favors condensation is observed for the onset of Bose-Einstein and multimode condensation, but in the regime of multimode condensation the behavior becomes more complicated and decondensation can be induced through an increase in pump rate $\Gamma_\uparrow$ or a decrease in thermalization coefficient γ. Given the extremely sensitive dependence of the system's phase on the excitation of dye molecules, there are several instances where small changes in pumping or thermalization result in a substantial redistribution of populations between the modes, and multiple triple and quadruple points.

Eventually, a critical assessment of experimental relevance is in order. Current experiments are performed for γ ranging between 0.2 and 5 and pump rates reach rates ten times the threshold value [27]. Exploring the upper half of the phase diagram presented in Fig. 2 requires substantially stronger pumping than currently realized. Since pulsed lasers can achieve peak pump rates 3 orders of magnitude higher than cw lasers, with pulse durations longer than the time taken to reach steady state, this seems a perfectly viable option.

Given the general applicability of the employed model, one can expect that multimode condensation and decondensation both inside and outside the lasing regime will be observable in plasmonic lattices coupled to dyes, which have recently shown condensation [38], semiconductors in photonic crystal resonators [39], and also more conventional laser systems. Exciton-polariton condensates (both semiconductor and organic), however, differ from photon condensates in that the mixed light-matter excitations relax directly through their matter component, whereas in photon and plasmon condensates equilibration occurs via exchanges between weakly coupled light and molecular excitations. Our predictions, therefore, do not translate directly, but it would be intriguing to identify similar mechanisms in these condensates.

The rich interplay between the different modes observed in Fig. 2 also offers great opportunities for the creation of tailored states of light [40], since the mode structure can easily be influenced through the shape of the cavity [28,41], lattice [38], or crystal structure [39], and the spatial pump profile can be varied. Since fluctuations are most relevant near phase transitions, we expect this rich phase diagram to be a fruitful tool in the search for unusual quantum correlations.

The data underlying this article are available at [34].

We acknowledge fruitful discussions with David Newman, Peter Kirton, and Jonathan Keeling, as well as financial support from the UK EPSRC [via a fellowship (Grant No. EP/J017027/1) and the Controlled Quantum Dynamics CDT Grant No. EP/L016524/1] and the ERC (via ODYCQUENT grant).

*r.nyman@imperial.ac.uk

[1] J. Bardeen, L. N. Cooper, and J. R. Schrieffer, Phys. Rev. **108**, 1175 (1957).
[2] M. Anderson, J. Ensher, M. Matthews, C. Wieman, and E. Cornell, Science **269**, 198 (1995).
[3] K. B. Davis, M.-O. Mewes, M. R. Andrews, N. J. van Druten, D. S. Durfee, D. M. Kurn, and W. Ketterle, Phys. Rev. Lett. **75**, 3969 (1995).
[4] S. Lübeck, Int. J. Mod. Phys. A **18**, 3977 (2004).
[5] W. Weidlich, Phys. Rep. **204**, 1 (1991).
[6] B. S. Kerner and H. Rehborn, Phys. Rev. Lett. **79**, 4030 (1997).
[7] J. Kasprzak, M. Richard, S. Kundermann, A. Baas, P. Jeambrun, J. Keeling, F. Marchetti, M. Szymańska, R. Andre, J. Staehli *et al.*, Nature (London) **443**, 409 (2006).
[8] H. Deng, D. Press, S. Götzinger, G. S. Solomon, R. Hey, K. H. Ploog, and Y. Yamamoto, Phys. Rev. Lett. **97**, 146402 (2006).
[9] R. Balili, V. Hartwell, D. Snoke, L. Pfeiffer, and K. West, Science **316**, 1007 (2007).
[10] J. D. Plumhof, T. Stöferle, L. Mai, U. Scherf, and R. F. Mahrt, Nat. Mater. **13**, 247 (2014).
[11] K. S. Daskalakis, S. A. Maier, R. Murray, and S. Kéna-Cohen, Nat. Mater. **13**, 271 (2014).
[12] H. Bernien, S. Schwartz, A. Keesling, H. Levine, A. Omran, H. Pichler, S. Choi, A. S. Zibrov, M. Endres, M. Greiner *et al.*, Nature (London) **551**, 579 (2017).
[13] J. Zhang, G. Pagano, P. W. Hess, A. Kyprianidis, P. Becker, H. Kaplan, A. V. Gorshkov, Z.-X. Gong, and C. Monroe, Nature (London) **551**, 601 (2017).
[14] P. Jurcevic, H. Shen, P. Hauke, C. Maier, T. Brydges, C. Hempel, B. P. Lanyon, M. Heyl, R. Blatt, and C. F. Roos, Phys. Rev. Lett. **119**, 080501 (2017).
[15] J. Zhang, F. M. Cucchietti, R. Laflamme, and D. Suter, New J. Phys. **19**, 043001 (2017).
[16] A.-W. de Leeuw, O. Onishchenko, R. A. Duine, and H. T. C. Stoof, Phys. Rev. A **91**, 033609 (2015).
[17] M. Fitzpatrick, N. M. Sundaresan, A. C. Y. Li, J. Koch, and A. A. Houck, Phys. Rev. X **7**, 011016 (2017).
[18] D. Sarchi, I. Carusotto, M. Wouters, and V. Savona, Phys. Rev. B **77**, 125324 (2008).
[19] J. M. Fink, A. Dombi, A. Vukics, A. Wallraff, and P. Domokos, Phys. Rev. X **7**, 011012 (2017).

[20] J. Klaers, J. Schmitt, F. Vewinger, and M. Weitz, Nature (London) **468**, 545 (2010).
[21] J. Klaers, F. Vewinger, and M. Weitz, Nat. Phys. **6**, 512 (2010).
[22] J. Schmitt, T. Damm, D. Dung, F. Vewinger, J. Klaers, and M. Weitz, Phys. Rev. A **92**, 011602 (2015).
[23] J. Marelic and R. A. Nyman, Phys. Rev. A **91**, 033813 (2015).
[24] J. Keeling and P. Kirton, Phys. Rev. A **93**, 013829 (2016).
[25] P. Kirton and J. Keeling, Phys. Rev. Lett. **111**, 100404 (2013).
[26] P. Kirton and J. Keeling, Phys. Rev. A **91**, 033826 (2015).
[27] J. Marelic, L. F. Zajiczek, H. J. Hesten, K. H. Leung, E. Y. X. Ong, F. Mintert, and R. A. Nyman, New J. Phys. **18**, 103012 (2016).
[28] B. T. Walker, L. C. Flatten, H. J. Hesten, F. Mintert, D. Hunger, J. M. Smith, and R. A. Nyman, arXiv:1711.11087.
[29] D. Vorberg, W. Wustmann, R. Ketzmerick, and A. Eckardt, Phys. Rev. Lett. **111**, 240405 (2013).
[30] C. Redlich, B. Lingnau, S. Holzinger, E. Schlottmann, S. Kreinberg, C. Schneider, M. Kamp, S. Höfling, J. Wolters, S. Reitzenstein, and K. Lüdge, New J. Phys. **18**, 063011 (2016).
[31] H. A. M. Leymann, D. Vorberg, T. Lettau, C. Hopfmann, C. Schneider, M. Kamp, S. Höfling, R. Ketzmerick, J. Wiersig, S. Reitzenstein, and A. Eckardt, Phys. Rev. X **7**, 021045 (2017).
[32] K. Michaelian and I. Santamaría-Holek, Europhys. Lett. **79**, 43001 (2007).
[33] The thermalization coefficient γ is directly related to the detuning, but since this relation depends on the absorption spectrum of the molecules there is no simple analytical form for it. Nevertheless, since γ is the more informative quantity, we will mostly refer to thermalization in the following.
[34] R. A. Nyman, 2017, https://doi.org/10.5281/zenodo.569817.
[35] See Supplementarl Material at http://link.aps.org/supplemental/10.1103/PhysRevLett.120.040601 for a detailed analysis and analytic solutions of the phase boundaries, the form of the absorption and emission spectra, a discussion of the threshold condition, and the effects of changing the pump width, which includes Ref. [36].
[36] D. Dung, C. Kurtscheid, T. Damm, J. Schmitt, F. Vewinger, M. Weitz, and J. Klaers, Nat. Photonics **11**, 565 (2017).
[37] The distinction we make here is that in Bose-Einstein and multimode condensate phases both absorption and emission play important roles, whereas (stimulated) emission dominates the behavior in the laser phase.
[38] T. K. Hakala, A. J. Moilanen, A. I. Vakevainen, R. Guo, J.-P. Martikainen, K. S. Daskalakis, H. T. Rekola, A. Julku, and P. Torma, arXiv:1706.01528.
[39] A.-W. de Leeuw, E. C. I. van der Wurff, R. A. Duine, D. van Oosten, and H. T. C. Stoof, Phys. Rev. A **94**, 013615 (2016).
[40] T. Hisch, M. Liertzer, D. Pogany, F. Mintert, and S. Rotter, Phys. Rev. Lett. **111**, 023902 (2013).
[41] L. Flatten, A. Trichet, and J. Smith, Laser Photonics Rev. **10**, 257 (2016).